Diamond & Related Materials 18 (2009) 1262–1266

Contents lists available at ScienceDirect

Diamond & Related Materials

journal homepage: www.elsevier.com/locate/diamond

Controlled synthesis and enhanced field emission characteristics of conical carbon nanotubular arrays

Santoshrupa Dumpala [a,1], Abdelilah Safir [b,1], David Mudd [c], Robert W. Cohn [b], Mahendra K. Sunkara [a], Gamini U. Sumanasekera [b,c,*]

[a] Department of Chemical Engineering, University of Louisville, Louisville, KY 40292, USA
[b] The Electro-Optics Research Institute and Nanotechnology Center, University of Louisville, Louisville, KY 40292, USA
[c] Department of Physics, University of Louisville, Louisville, KY 40292, USA

ARTICLE INFO

Article history:
Received 21 February 2009
Received in revised form 7 April 2009
Accepted 28 April 2009
Available online 3 May 2009

ABSTRACT

Conical carbon nanotubes (CCNTs) with unique structural characteristics arising from their tapered morphologies compared to uniform diameter carbon nanotubes, have been shown to exhibit enhanced field emission properties and support high current densities. Specifically, several CCNT arrays with different morphological characteristics (tip radius, aspect ratio, density and wall structure) were synthesized by variations in the process parameters using a microwave plasma chemical vapor deposition (MWCVD) reactor. The field emission characteristics for a CCNT array sample with a tip radius of 5 nm, density of $10^8/cm^2$ and having the highest aspect ratio exhibited a low turn-on electric field (<0.7 V/μm) and a high field enhancement factor (β>7500). Other samples with lower emission characteristics were attributed either to the presence of field screening effect resulting from higher CCNT density or due to the corresponding tip and wall characteristics.

1. Introduction

Field emission from carbon nanotubes (CNTs) has been explored for potential applications varying from flat panel displays to miniature scanning electron microscope columns [1]. CNTs are known to possess most of the favorable properties as field emitters such as high aspect ratio, good mechanical, electrical, thermal and chemical properties, and ability to be grown as vertical arrays with controlled density [2,3]. The dependence of field emission properties of carbon nanotubes on (i) diameter (ii) length (iii) density/sparsity (spacing between neighboring tubes) (iv) alignment/randomness, (v) wall defects, and (vi) surface absorbates has been explored to a greater depth [4]. Higher values of β result in higher local electric field (low turn-on fields) as well as current densities, which is extremely desirable in many applications such as X-ray devices. Although higher β values (2500–10,000) and lower turn-on fields (0.8–1.5 V/μm) have been reported for single walled nanotubes (SWNTs) and multi walled nanotubes (MWNTs) [5–7], the lower current densities (10 mA/cm^2) limit their applicability as efficient cold cathodes for applications in electron and X-ray sources. Considering these limitations, new morphological structures with excellent field emission properties are highly desired.

Recently, conical carbon nanotubes (CCNTs) essentially consisting of central carbon nanotube surrounded by helical graphene sheets, known as either "carbon nanopipettes" (CNPs) [8] or "tubular graphite cones" (TGC) [9] have been synthesized by microwave plasma chemical vapor deposition (MWCVD). Long CCNTs grown vertically with moderate densities, together with their tapered morphologies can be well separated at their tips [10], which in turn contribute to the reduction of field screening effect provoked by the proximity of neighboring structures when the arrays are used as field emitters. In fact, the inter-emitter distance should be at least 1–2 times the emitter length to minimize the field screening effect [11]. Tapered emitters are expected to be mechanically more stable than a constant diameter nanotube of the same tip diameter. Also tapered structures, due to their increasing cross sectional area away from the tip, increase the thermal transport and are likely to sustain greater current densities than nanotubes. Field emission measurements on CCNTs grown with metal catalysts have been reported [12,13]. However, the extent of the above studies is limited and the structures studied do not represent the ideal conical morphology due to the presence of metal contamination at their tip. In the present work, several CCNT array samples were synthesized by adjusting growth

* Corresponding author. Department of Physics, University of Louisville, Louisville, KY 40292, USA.
E-mail address: gusuma01@gwise.louisville.edu (G.U. Sumanasekera).
[1] Authors contributed equally to this work.

0925-9635/$ – see front matter © 2009 Elsevier B.V. All rights reserved.
doi:10.1016/j.diamond.2009.04.004

Table 1
Experimental conditions, the resulting structural characteristics, and the field emission properties of the three CCNT array samples used in this study.

Sample #	Experimental conditions			Structural properties			Field emission properties		
	Process time (min)		Power (W)	Density (10^8/cm^2)	Average length (l) (μm)	Average radius (r) (nm)	β_{max} [a]	E_T [b] (V/μm)	I_{max} [c] (μA)
	Step 1	Step 2							
1	120	150	900	2.2	9.0 ± 0.1	5 ± 1	7600	0.66	520
2	30	165	980	4.5	7.0 ± 0.1	13 ± 1	2313	1.5	320
3	15	165	980	0.7	4.0 ± 0.1	12 ± 1	1324	2.3	200

[a] Maximum field enhancement factor measured.
[b] Lowest measured turn-on electric field.
[c] Maximum current corresponding to threshold electric field of 3.6 V/μm.

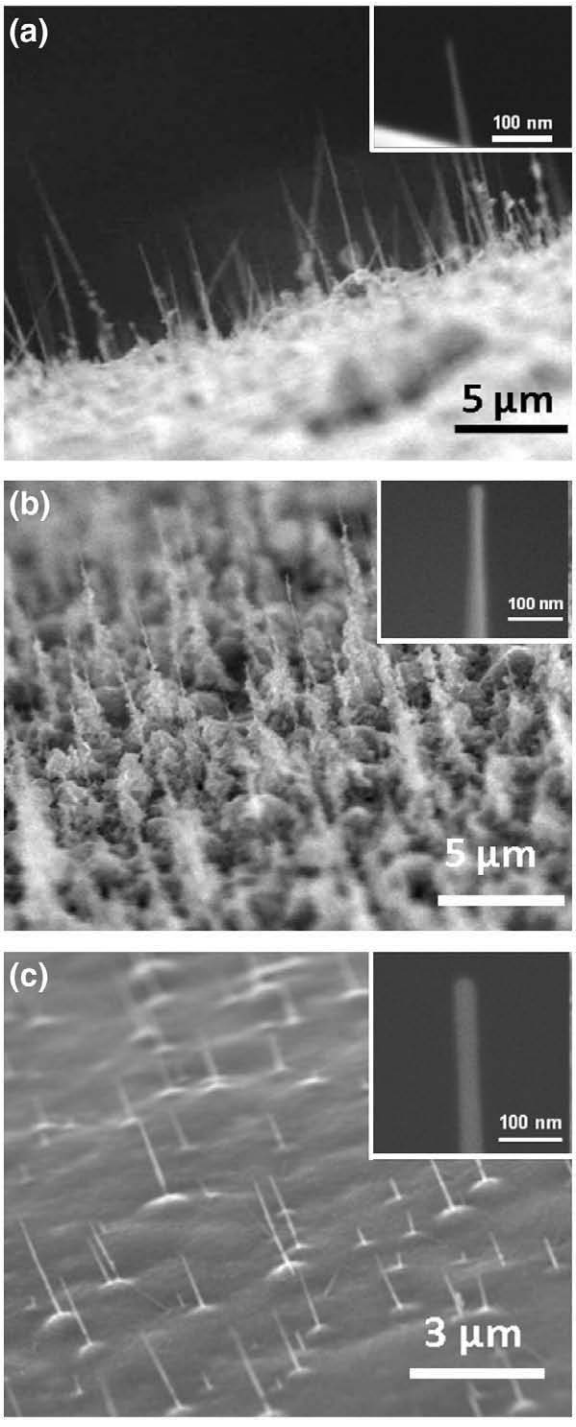

Fig. 1. SEM images of array of CCNTs of (a) sample 1 (b) sample 2 and (c) sample 3, with insets showing the enlarged view of the corresponding CCNT tip.

parameters that control aspect ratio, density and wall structures. The results show that the performance of the CCNT arrays is dependent upon their morphology and can match or exceed that reported for SWNTs and MWNTs [5–7].

2. Experimental

Five different samples of CCNT arrays were grown on platinum wires (300 μm diameter) using a MWCVD reactor (ASTeX 5010, 3.5 kW) at a pressure of 24 Torr and 950 W power. The platinum wires were vertically placed on a graphite susceptor inside the reactor. The experimental procedure was similar to that of a previous work [8], except the addition of a two step process with a change in the gas phase composition to vary the structural characteristics of CCNTs. Step 1 consists of carbon deposition using 1.35 vol.% methane in 200 sccm of hydrogen followed by a deposition and etching with 1 vol.% methane in step 2.

Field emission measurements were performed on each sample in a vacuum chamber at a pressure of 10^{-7} Torr. The platinum wire with as-synthesized CCNTs was placed in a V-groove of a copper plate. A flat copper anode was moved towards the CCNTs by means of a micro manipulator. A zero inter-electrode distance ($d = 0$) was established by observing a sudden change in resistance when the anode touches the CCNTs. Measurements were performed at 5 different distances (d) by sweeping the voltage from 0 to 500 V while recording the current using a Keithley 6487 pico-ammeter equipped with a built in variable voltage source.

3. Results and discussions

The variation in time scales used for both the process steps during the synthesis of CCNTs resulted in variation in the density, length and the morphology of the CCNT arrays. The experimental conditions employed and the resulting CCNT characteristics for samples 1–3 were summarized in Table 1. Increase in the time of step 1 increases the density and length, with ~80% of the CCNTs within a few 100 nm of their average length. Increasing the duration of step 2 increases the etching of the CCNTs and also reduces the density of CCNTs. Fig. 1 shows the SEM images of these three samples of CCNT arrays grown on a platinum wire. The corresponding insets present the enlarged view of individual CCNT tips, which show the absence of any metal catalyst at the tip.

Fig. 2 shows the SEM images of the individual CCNT of these three samples clearly depicting the variations in the wall structure and morphology. Sample 1 with the longest carbon deposition step, has CCNTs with the highest aspect ratio (Fig. 2(a)), moderate density and also the smallest tip radius estimated from SEM image characterization based on Fig. 1 indicated in Table 1. Sample 2 has CCNTs with lower aspect ratio and larger tip diameter than sample 1, in addition to the presence of carbon flakes along the length of each CCNT as depicted in Fig. 2(b). Sample 3 with longer etching step and a shorter deposition time resulted in CCNTs with the lowest aspect ratio and uneven etching as clearly seen in Fig. 2(c). CCNTs of sample 1 with small tip radius, optimum density and high aspect ratio accounts for

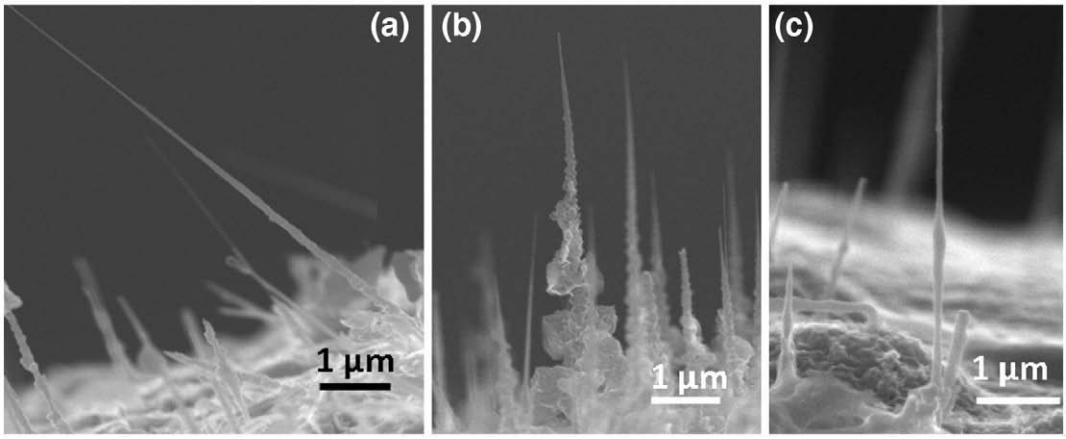

Fig. 2. SEM images of the individual CCNT of (a) sample 1 (b) sample 2 and (c) sample 3, illustrating the variation in the wall structure and aspect ratio.

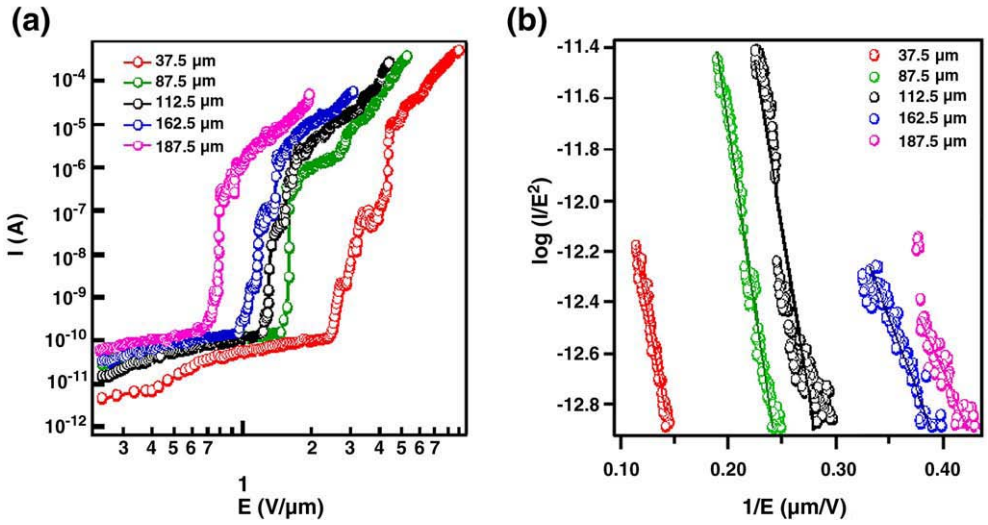

Fig. 3. Field emission properties from the CCNTs showing the plots of (a) Current vs. the macroscopic electric field for various inter-electrode distances (d) for sample 1, (b) corresponding F-N plots.

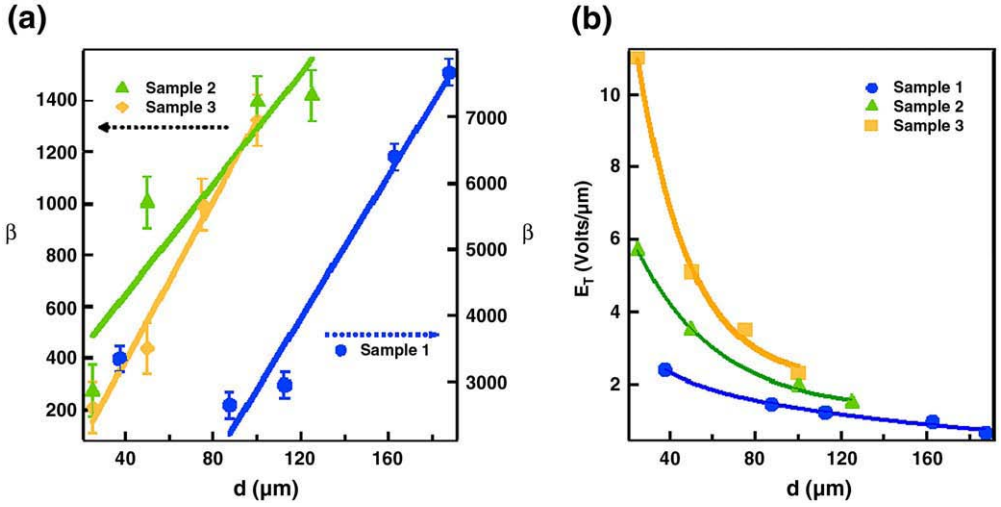

Fig. 4. Plots of (a) field enhancement factor β and (b) turn-on electric field as a function of distance for samples 1–3.

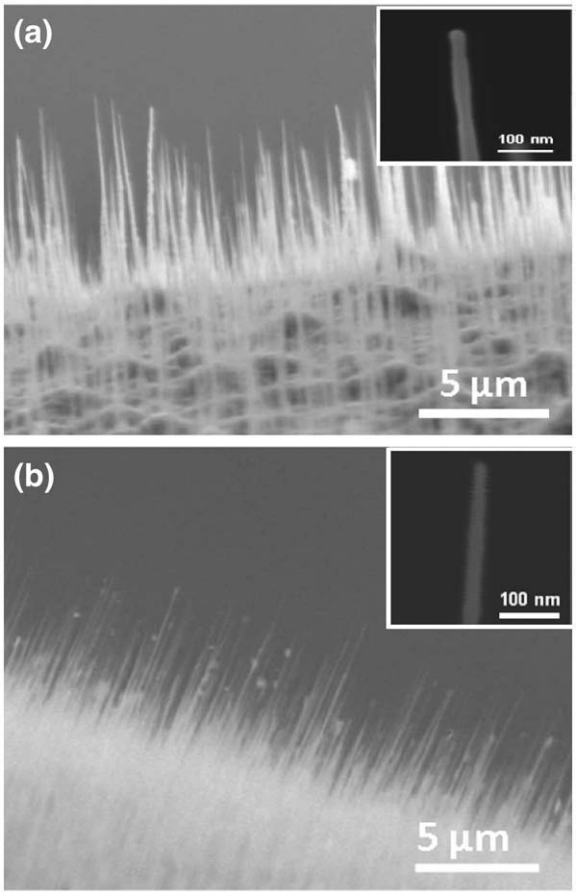

Fig. 5. SEM images of CCNT arrays of (a) sample 4 (b) sample 5, with insets showing the enlarged view of the corresponding CCNT tip.

the enhanced field emission characteristics as described in the following analysis.

Current (I) is measured as a function of applied electric field ($E = V/d$) for sample 1 at each of the five inter-electrode distances (d) as shown in Fig. 3(a). According to the Folwer–Nordheim (F-N) equation the electric field (E_{eff}) at the tip of CCNT produces emission current density (J):

$$J = \frac{A(E_{\text{eff}})^2}{\phi} e^{-\left(\frac{B\phi^{3/2}}{E_{\text{eff}}}\right)} \quad (1)$$

where ϕ is the work function of the emitter in electron volts (eV) (typically chosen to be 5 eV in the present case and other sp^2 carbon materials [12]), $A = 1.56 \times 10^{-6}$ A V^{-2} eV, and $B = 6.83 \times 10^9$ V (eV)$^{-3/2}$ m^{-1}. Fig. 3(b) shows the corresponding F-N plots of $\ln(I/E^2)$ vs. $1/E$ at each d value. This plot represents the emission current region between the two knees of Fig. 3(a). The linearity of the plot is indicative of the field emission in the operating current regimes. The slope of this linear plot is given by $\left(\frac{B\phi^{3/2}}{\beta}\right)$, where β is the field enhancement factor, defined as $E_{\text{eff}} = \beta E_{\text{appl}}$ where, E_{appl} is the applied electric field and E_{eff} is the effective field at the emission point.

Fig. 3(a) shows that the current begins to saturate at a second knee for sample 1. This observed saturation may be associated with heat induced changes at the tip [18,19]. The maximum electric field reported for multiwall carbon nanotubes is ~8 V/nm before undergoing tip failure (due to deformation, evaporation, thermal runaway or arcing) [14,15]. The estimation of the current density in our samples is complicated by the curved platinum support. However, we have reached the effective electric field (βE_{app}) ~8 V/nm achieving current densities greater than 3 A/cm^2 at the second knee for sample 1 at a distance of 187.5 µm, without experiencing thermal runaway.

Of the three samples, sample 1 has the highest β value of 7600 as shown in Fig. 3(c) which enables the CCNT array to continue to emit up to $d = 187.5$ µm (for the maximum source voltage available). This high value of β is due to a combination of factors such as small radius of curvature at the tip, high aspect ratio, moderate emitter density of CCNTs in sample 1 and the increased distance (d). In the previous study on CCNTs terminated with nickel catalyst particles, the field enhancement factor as low as 80 have been reported [12]. The value of β for samples 2 and 3 ranges from 2000 to 3000. Sample 3 has the poorest emission properties of three samples due to the formation of amorphous carbon along the side walls of CCNT resulting from the prolonged etching which minimizes the edge plane emission sites [16]. Fig. 4(a) shows a linear dependence of experimentally derived β on d, plotted for each of the three samples. The value of β determined by field emission study is large compared to the geometrical enhancement

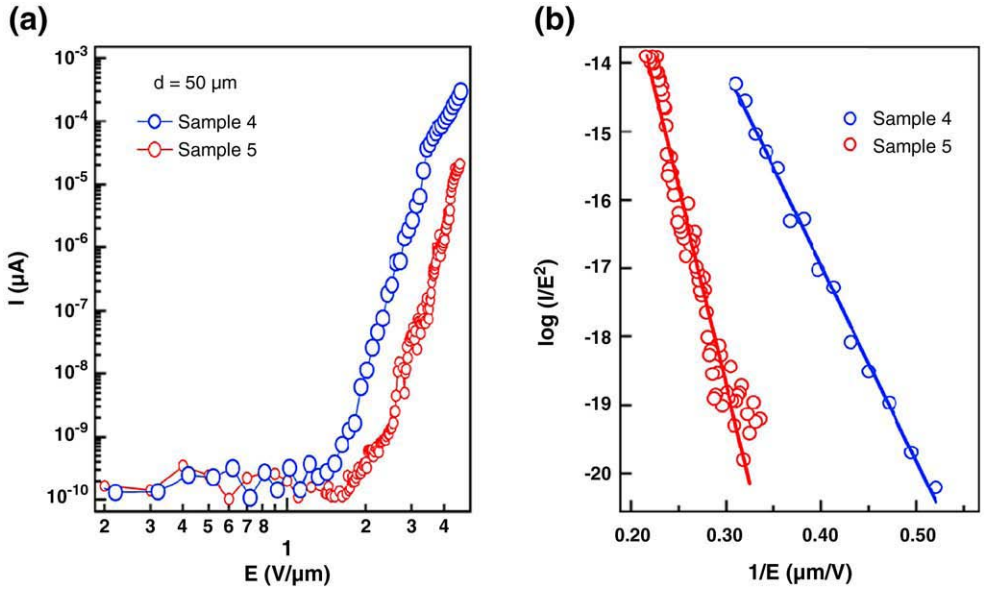

Fig. 6. Field emission properties from the CCNTs showing the plots of (a) Current vs. the macroscopic electric field for sample 4 and sample 5, (b) corresponding F-N plots.

Table 2
Comparison of the resulting structural characteristics, and the field emission properties of the two morphologically similar but with different density CCNTs array samples.

Sample #	Structural properties			Field emission properties		
	Density (10^8/cm^2)	Average length (l) (μm)	Average radius (r) (nm)	β_{max} [a]	E_T [b] (V/μm)	I_{max} [c] (μA)
4	15	7.0 ± 0.1	12 ± 1	2920	1.72	307
5	20	7.0 ± 0.1	11 ± 1	1424	2.2	20

[a] Maximum field enhancement factor measured.
[b] Lowest measured turn-on electric field.
[c] Maximum current corresponding to threshold electric field of 3.6 V/μm.

factor given by h/r, where h is the length of the CCNT and r is the radius of curvature at the tip. This deviation was also observed earlier for highly dense carbon nanotube arrays which demonstrated that β depends on the inter-electrode distance (d) and other factors such as tip radius, aspect ratio [17] and field screening effect [11]. In the present case this discrepancy can be attributed to the structural characteristics of these conical morphologies with open edges on the outer surface acting as emission sites. The effects of the surface adsorbates also cannot be ruled out [18]. Fig. 4(b) shows that turn-on electric field (E_T, electric field corresponding to emission current of 1 nA) decreases with increasing distance (d) for all three samples, reaching a value as low as 0.7 V/μm (Fig. 3(a)) for sample 1 at the maximum possible separation distance, which can be accounted for the high β value. This low turn-on electric field, value is comparable to the best values reported for SWNTs and MWNTs [5–7].

Table 1 illustrates the experimental conditions, the resulting structural and the field emission properties of the three CNP array samples used in this study. Experimental conditions consist of the growth process time and the microwave power employed for the synthesis of all five CCNT samples. Structural characteristics include the average length, estimated density, and the average radius of curvature at the tip of each CCNT sample from SEM image analysis. This section includes the maximum β, the lowest E_T, the maximum emission current per single CCNT.

Out of five samples, samples 4 and 5 were varied only in the CCNTs density while other structural characteristics such as length, radius of curvature at the tip and wall structure were maintained the same. Fig. 5 shows the SEM images of (a) sample 4 and (b) sample 5 where the increased density of sample 5 is clearly seen. As illustrated in Fig. 6 sample 4 has better emission properties compared to sample 5, which can be attributed to the reduced field screening affect from the neighboring emitters due to lower density. The structural and emission characteristics of both the samples are shown in Table 2.

4. Conclusions

In summary, we successfully synthesized the CCNT samples with different densities, radii of curvatures, lengths and wall structures by varying the critical growth parameters. Field emission studies on these conical structures resulted in a turn-on electric field as low as 0.7 V/μm and field enhancement factor as high as 7600. We also showed that not only did the characteristic features of emitter such as high aspect ratio, small radius of curvature at the tip, enhance the field emission properties, but also optimum emitter density plays an important role in reducing the field screening effect. With controlled aspect ratio, density, and uniformity; CCNTs can be turned into potential field emitters and next generation cold cathode field emitters.

Acknowledgements

This study was supported by the U.S. Department of Energy (DE-FG02-05ER64071, DE-FG02-07ER46375) and the Kentucky NASA EPSCoR.

References

[1] Z. Chen, Y. Wei, C.X. Luo, K.L. Jiang, L. Zhang, Q.Q. Li, S.S. Fan, J.C. Gao, Appl. Phys. Lett. 90 (2007) 1331081.
[2] S. Fujii, S. Honda, H. Machida, H. Kawai, K. Ishida, M. Katayama, H. Furuta, T. Hirao, K. Oura, Appl. Phys. Lett. 90 (2007) 153108.
[3] W.I. Milne, K.B.K. Teo, G.A.J. Amaratunga, P. Legagneux, L. Gangloff, J.P. Schnell, V. Semet, V.T. Binh, O.J. Groening, Mater. Chem. 14 (2004) 933.
[4] J.M. Bonard, H. Kind, T. Stockli, L.A. Nilsson, Solid-State Electron. 45 (2001) 893.
[5] J.M. Bonard, J.P. Salvetat, T. Stöckli, W.A. de Heer, L. Forró, A. Châtelain, Appl. Phys. Lett. 73 (1998) 918.
[6] Q.H. Wang, T.D. Corrigan, J.Y. Dai, R.P.H. Chang, A.R. Krauss, Appl. Phys. Lett. 70 (1997) 3308.
[7] M. Sveningsson, R.E. Morjan, O.A. Nerushev, Y. Sato, J. Backstrom, E.E.B. Campbell, F. Rohmund, Appl. Phys., A Mater. Sci. Process. 73 (2001) 409.
[8] R.C. Mani, X. Li, M.K. Sunkara, K. Rajan, Nano Lett. 3 (2003) 671.
[9] G.Y. Zhang, X. Jiang, E.G. Wang, Science 300 (2003) 472.
[10] R.D. Lowe, R.C. Mani, R.P. Baldwin, M.K. Sunkara, Electrochem. Solid-State Lett. 9 (2006) H43.
[11] L. Nilsson, O. Groening, C. Emmenegger, O. Kuettel, E. Schaller, L. Schlapbach, H. Kind, J.M. Bonard, K. Kern, Appl. Phys. Lett. 76 (2000) 2071.
[12] W. Zhang, Z.H. Xi, G.M. Zhang, S. Wang, M.S. Wang, J.Y. Wang, Z.Q. Xue, Appl. Phys., A Mater. Sci. Process. 86 (2007) 171.
[13] J.J. Li, C.Z. Gu, Q. Wang, P. Xu, Z.L. Wang, Z. Xu, X.D. Bai, Appl. Phys. Lett. 87 (2005) 143107.
[14] M.S. Wang, Q. Chen, L.M. Peng, Small 4 (2008) 1907.
[15] K.A. Dean, T.P. Burgin, B.R. Chalamala, Appl. Phys. Lett. 79 (2001) 1873.
[16] B. Chernomordik, S. Dumpala, Z.Q. Chen, M.K. Sunkara, Chem. Vap. Depos. 14 (2008) 1.
[17] N.S. Xu, Y. Chen, S.Z. Deng, J. Chen, X.C. Ma, E.G. Wang, J. Phys., D. Appl. Phys. 34 (2001) 1597.
[18] A. Maiti, J. Andzelm, N. Tanpipat, P. von Allmen, Phys. Rev. Lett. 87 (2001) 155502.